PIV measurement of particle motion in spiral gas–solid two-phase flow

Kaoru Miyazaki [a], Gang Chen [b], Fujio Yamamoto [c], Jun-ichi Ohta [c], Yuichi Murai [c], Kiyoshi Horii [d]

[a] *Copros Company, Simonoseki-shi, Yamaguchi, 752-0962, Japan*
[b] *Xian University of Technology, Xian, 710048, People's Republic of China*
[c] *Department of Mechanical Engineering, Fukui University, Fukui-shi, 910-8507, Japan*
[d] *Shirayuri Women's College, Tokyo, 182-8525, Japan*

Abstract

With a concise review on some basic and novel algorithms and methods for the techniques of particle-imaging velocimetry (PIV), the paper reports an application of the PIV techniques to the investigation of particle motion in a gas–solid two-phase spiral flow in a horizontal tube. Axial velocities of the transported particles are obtained. Some important features of particle motion governing high transportation efficiency of the spiral flow are revealed by investigating probability density distribution of particle locations in a pipe cross-section.

Keywords: Particle-imaging velocimetry; Gas–solid two-phase flow; Spiral flow; Pipe transportation

1. Introduction

Particle-imaging velocimetry (PIV in acronym) has been rapidly developed and used to measure instantaneous velocity vector fields from slow flows to supersonic flows during the past 10 years [1–3]. In contrast to other methods for one-point measurements such as the Pitot tube, the hot wire anemometer and the laser Doppler velocimeter, PIV can carry out two-dimensional and three-dimensional instantaneous velocity measurement. Physical information such as pressure field and vorticity field can be extracted based on the velocity vector map obtained from PIV. A survey paper of particle velocimetry confirms that PIV has been rapidly advanced in its fundamentals and applications to multiphase flows, thermal flows, turbulence structures, etc. [4]. The PIV techniques are applied to the investigation of particle motion in pneumatic transportation in the present study.

Pneumatic transportation of solid particles is widely used in many types of industrial pipelines. It has been found that an improved method using a spiral-flow-generating nozzle can decrease the power consumption and increase the distance of soil transportation in a sewage pipe installation system. The higher efficiency of the transportation system has been obtained with the spiral-flow method. The reason of the efficiency improvement is considered to be due to a reduction of particle–pipe friction. Therefore, the probability distribution of the particle locations and the particle velocities are measured and analyzed by applying the PIV together with image processing techniques. In this paper, some useful results obtained from the PIV measurement of the gas–solid two-phase spiral flow are reported alongside a concise review of the techniques of PIV.

2. Current PIV techniques

In previous papers, the method acquiring velocities at grid points using high-density distribution patterns of particle images is referred to as PIV, and the method using each particle tracking for low particle number density is usually referred to as particle tracking velocimetry (PTV

in acronym). In this paper, PIV is used as a general term for velocimetry using particle images. When particles have a good behavior of traceability to a fluid flow, the particle velocities usually represent the local fluid velocities. If the particles do not follow the flow, the particle velocities do not represent the local fluid velocities. For instance, gas flows faster than solid particles in the spiral gas–solid two-phase flow that we discuss in this paper. This difference of velocities between fluid and particles makes all the PIV techniques, especially their algorithms, not always applicable to an investigation into the motion of particles, drops and bubbles in a multiphase flow system. The PIV techniques are concisely reviewed before introducing the PIV measurement of particle motion in the present spiral gas–solid two-phase flow, although the gas velocity is not measured.

The authors classify the current types of PIV techniques according to principles of flow velocity calculation based on the image processing. Under this viewpoint, principles and features of some current PIV techniques are listed in Table 1.

The algorithm of particle brightness-distribution pattern tracking shown in Table 1 is the most popular method. Correct pairs of elements of particle clouds are obtained in two consecutive frames based on the similarity of image brightness distribution patterns in the two frames by calculating the values of cross-correlation coefficients defined by Eqs. (1) or (2) [1]. The similarity of image-brightness distribution patterns may also be evaluated by the method of the minimum quadratic difference defined by Eq. (3) [9] or by the method of summation of absolute value of brightness differences defined by Eq. (4) [10]. In these equations, f_{ij} and g_{ij} are digital gray values of the pixels in overlapping interrogation windows of size $M \times N$ pixels which consist of elements of particle clouds in two consecutive frames, whereas $\bar{f}$ and $\bar{g}$ are the mean values of brightness in the interrogation windows. When the maximum value of C_{fg}, or the minimum value of A_{fg} or B_{fg} are found for a pair of the two interrogation windows, the pair is considered to be identified. The velocity of the particle clouds is computed by using the displacement of the cloud center and the time interval Δt between the two frames.

$$C_{fg} = \frac{\sum_{i=1}^{N}\sum_{j=1}^{M} f_{ij}g_{ij}}{\sqrt{\sum_{i=1}^{N}\sum_{j=1}^{M} f_{ij}^2 \cdot \sum_{i=1}^{N}\sum_{j=1}^{M} g_{ij}^2}}, \tag{1}$$

$$C_{f-\bar{f}\,g-\bar{g}} = \frac{\sum_{i=1}^{N}\sum_{j=1}^{M}(f_{ij}-\bar{f})(g_{ij}-\bar{g})}{\sqrt{\sum_{i=1}^{N}\sum_{j=1}^{M}(f_{ij}-\bar{f})^2 \sum_{i=1}^{N}\sum_{j=1}^{M}(g_{ij}-\bar{g})^2}}, \tag{2}$$

$$A_{fg} = \frac{1}{NM}\sum_{i=1}^{N}\sum_{j=1}^{M}(f_{ij}-g_{ij})^2, \tag{3}$$

$$B_{fg} = \sum_{i=1}^{N}\sum_{j=1}^{M}|f_{ij}-g_{ij}|. \tag{4}$$

Another kind of technique employs the algorithm of particle distribution pattern tracking. Each particle motion is tracked and the particle velocity is calculated from the displacement of the particle center between the two consecutive frames [11,12]. This is called binary image cross-correlation method (BICC), using the binarized images of two consecutive frames for a high-speed calculation. The computation of the value of cross-correlation given by Eq. (1) can be simplified as the following equation after a mathematical discussion [13]:

$$C_{fg} = \frac{L}{\sqrt{nm}}, \tag{5}$$

where L is the summation of logical products of the image brightness binarized with the value of 1 or 0 at each pixel in two overlapping interrogation windows for two consecutive frames, whereas m and n are numbers of bright pixels in the first and second windows, respectively. The computation time of Eq. (5) is much shorter than that of Eq. (1) or (2). Therefore, the method of BICC is able to achieve a real time measurement of the flow velocity field. The method is, however, limited to the case of low number density of particles.

Another method of particle distribution pattern tracking is a so-called Delaunay tessellation technique [14] which also uses two consecutive binarized images. The similarity of the two Delaunay triangles consisting of three centroids of particle images in each of the two pictures instead of the interrogation windows is evaluated by the following equation:

$$T = \frac{\text{Area}(\text{TR1} \cap \text{TR2})}{\sqrt{\text{Area}(\text{TR1}) \cdot \text{Area}(\text{TR2})}}, \tag{6}$$

where Area(TR1 ∩ TR2) stands for overlapping area of triangles TR1 and TR2, Area (TR1) is the area of triangle TR1 and Area(TR2) is that of triangle TR2. This technique has a much higher performance speed than the method of BICC, and can obtain information of fluid rotation together with translation velocity. Spurious vectors, which appear in the pattern tracking methods, can also be more effectively decreased by the technique of the Delaunay triangle. However, computation work by this method will be extremely large when extended to measurement of three-dimensional flow.

The last kind of method listed in Table 1 is based on particle trajectory tracking, frequently called PTV [17–20]. The principle of the trajectory tracking algorithm is based on an evaluation of the smoothness of particle trajectory. A method for evaluating the smoothness employs the change in direction of particle trajectory in two consecutive frames [17]. The second method evaluates the deviation of combined changes in particle displacement and direction in four consecutive frames [18] and is named 4-PTV in this paper. Then there is the third algorithm that evaluates the changes in acceleration based on four consecutive frames [19]. When the

Table 1
Some current particle image velocimetry techniques

Classifications	Principles	Features and merits	Limits	Remarks
Pathline [5,6]	Measurement of particle pathline length	Simple	High cost for ambiguity removal Low image density	Not suitable to automatic measurement of large scale data
Laser speckle velocimetry [7,8] (LSV)	Young's fringe in optical specklegram	Small computation in automatic evaluation system Applicable to high speed flow	More particles are needed [1] Direction ambiguity [3]	Difficult in three-dimensional flow
Particle brightness-distribution pattern tracking	Maximum value of cross-correlation coefficient [1]	Two frames High image density	2*D* Large computation	Most popular
	Minimum quadratic difference [9]	Two-frames High image density	2*D*	
	Minimum sum of absolute value of brightness difference [10]	Two-frames High image density	2*D*	
Particle distribution pattern tracking	Maximum value of binary image cross-correlation coefficient [11–13]	Two frames High-speed algorithm 2*D* and 3*D*	Low image density	
	Maximum value of Delaunay triangle similarity coefficient [14]	Two frames High-speed algorithm Applicable to rotation	Low image density 2*D*	Delaunay tessellation is unique and optimal triangle
Spring model	Minimum force in imaginary spring systems [15]	Two frames 2*D* and 3*D* Applicable to shear and rotation	Low image density	
Velocity gradient tensor method	Minimum value of a sum of squared particle distance [16]	Two frames 2*D* and 3*D* Applicable to shear and rotation	Low image density	
Particle trajectory tracking	Matching probability (particles in a small region moving towards nearly the same direction) [17]	Two frames	Low image density 2*D*	
	Smooth trajectories [18]	Four frames 2*D* and 3*D*	Low image density	Less spurious vectors
	Minimum change in acceleration [19]	Four frames 3*D*	Low image density	

particle number density is so low that the spacing between particles is large compared with the displacements of the particles between exposures, pairs of images are easily recognized and any special algorithm for trajectory tracking is no longer necessary. This is the simplest case for particle identification with PIV techniques [20] and named 2-PTV in this paper.

Spurious vectors may appear in the velocity vector field from PIV measurements due to the mis-matching of particle pair. In this case, some disposals such as detection and removal of spurious vectors, and replacement of spurious vectors by correct ones are taken [21–25]. Firstly, noise signals should be avoided in the process of image recording by controlling illumination, seeding and recording devices carefully. Secondly, noise should be removed during the image processing for calculating brightness, coordinates, areas and centroids of particle images. At last spurious vectors in the measured velocity vector field should be removed by some special methods [12,14]. In a gas–solid two-phase flow, it is more difficult to delete spurious velocity vectors of the solid phase because the continuity equation of fluid flow cannot be applied to the solid phase. As a possible technique for three-dimensional measurement with minimum amounts of spurious velocity vectors, the PTV is a good choice for investigating the behavior of particles or drops in a multiphase system. The 2-PTV and 4-PTV techniques, which track each particle trajectory smoothly in two and four consecutive frames, respectively, are used for the investigation of particle motion in the present gas–solid two-phase spiral flow.

3. Application of PIV to gas–solid spiral flow

3.1. The spiral air flow

The spiral flow is generated by a spiral nozzle, which has been described in previous papers [26,27] and holds a patent (China Patent No. 23648). Differing from other forced swirls, which are conventionally

produced by adjustable vanes, tangential injection, flow through a rotating perforated plate and flow in a long rotating tube, the spiral flow has a steeper-mountain type axial velocity profile than the other swirls that have a valley type of axial velocity profile. The spiral flow has been applied successfully to orientation control in high-performance installation of optical fiber [28], to the plasma deposition in pipe [29], dispersion and encapsulation of submicron powders [30]. Especially much longer transportation distance was achieved by making use of the spiral nozzle for the installation of optical fibers [31].

As shown in Fig. 1, the nozzle is provided with an annular slit connected to a conical cylinder. Pressurized air without intentionally designed azimuthal flow is supplied through this slit, and the air passing through the conical cylinder with a Coanda surface changes into a spiral flow. It is considered that the spiral flow is generated by the total effects of flow instability of the annular jet and Coanda effect of the conical cylinder. It is known that spiral strength was effected by the slit angle α in Fig. 1.

Recently, the authors have begun to apply the air spiral flow to the transportation of soil particles in a sewage pipe installation system and found that power consumption of the system is reduced by 50% and transportation distance is increased by 40% using the spiral nozzle [32]. In order to elucidate the reason why such high transportation performance can be realized in the spiral gas–solid two-phase flow, the particle migration features are investigated by using the techniques of 2-PTV and 4-PTV.

3.2. *Experimental apparatus and image capturing*

A schematic diagram of the experimental apparatus is shown in Fig. 2. Solid particles, i.e. glass beads with a density of 2500 kg/m^3, are fed to the spiral nozzle and driven into the transportation pipe. The diameters of the beads are 2.9–3.9 mm. The transportation pipe is an acrylic pipe with an internal diameter of $D = 22$ mm and a length of 5.5 m. The Reynolds number of air flow is 3.95×10^4 based on the pipe diameter and the mean velocity of the air flow, which is evaluated to about 26.5 m/s from the measurement of Pitot tube. Measurement sections for the particle motion are located at distances of $20D$ and $200D$ from the nozzle exit.

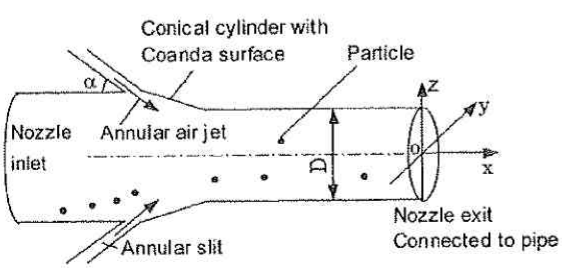

Fig. 1. Schematic diagram of the spiral nozzle.

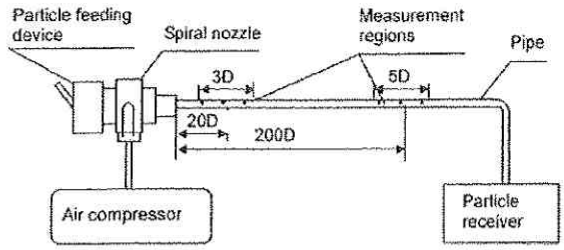

Fig. 2. Sketch of the transportation facility.

Particle images in three-dimensional space are recorded by a charge-coupled device (CCD) camera, and particle coordinates are obtained by processing the recorded particle images. The images should be clear for taking out particle coordinates. Axial displacements of particle centroids can be calculated from two consecutive frames in 2-PTV and four consecutive frames in 4-PTV. A mirror inclined at an angle of 45° relative to the horizontal plane was used to calculate the y-coordinate of particle position in the pipe cross-section, i.e. in the y–z plane at axial coordinate x. A conceptual diagram is shown in Fig. 3, where the image of a particle p is taken at $p1$ in the mirror. The y-coordinate $y(p)$ of the particle p can be calculated by the following equation:

$$y(p) = y1(p1) \times MA(y(p)), \tag{7}$$

where $MA(y(p))$ is magnification, which was determined by calibrating the camera parameters before photographing [33].

An arrangement of the present PIV system is shown in Fig. 4. It is made up of an illumination system, a CCD camera and a personal computer (Machintosh 7500/100) with a built-in image processor for getting binary images, software for calculating coordinates of particle

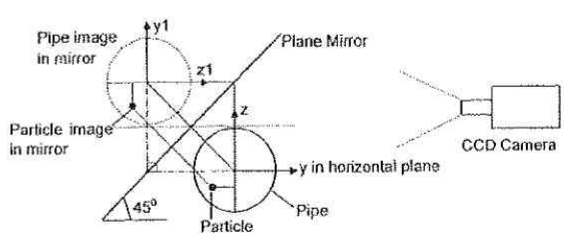

Fig. 3. Conceptual diagram of the photographing method.

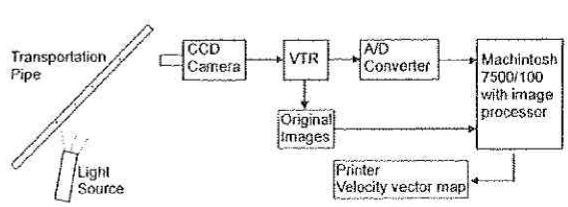

Fig. 4. Arrangement of the PTV system.

pairs and particle velocities. The original images were recorded by a high-speed camera with 640×480 pixels (NAC HSV-1000).

3.3. Axial velocities of particles

Averaged axial velocities of particles are an important parameter for the present flow in the pipeline. Based on the measured particle-averaged axial velocity and the particle number flow rate, the particle number density in the pipe can be estimated. In other cases, the averaged axial velocity and the particle number density are measured, finally calculating the particle flow rate.

When the particle number density is low enough, 2-PTV was used [20]. In our measurements, a CCD camera with shutter speed 500 frames per second was used for stereoscopic imaging of a particle. The averaged axial velocity of particles is given by the following equation:

$$\bar{u}_p = \frac{1}{n}\sum_{i=1}^{n}\frac{\Delta x_i}{\Delta t}, \tag{8}$$

where Δx_i is the axial displacement of a particle i at a time interval $\Delta t = 1/500$ s, and n is the total particle number in chosen frames.

Measured axial velocities of particles are shown in Figs. 5–7 for nozzles of $\alpha = 30°$, 60° and 90°, respectively, in order to observe the effect of slit angle of the nozzle. In the measurement section at $x/D = 20$, the averaged particle velocity of $\bar{u}_p = 7.3$ m/s for the nozzle of $\alpha = 30°$ is about 15% higher than that of $\bar{u}_p = 6.3$ m/s for the nozzle $\alpha = 0°$ and $\bar{u}_p = 6.4$ m/s for the nozzle $\alpha = 90°$. This means the former makes larger acceleration. In the section of $x/D = 200$, however, the detected particle-averaged axial velocities of $\bar{u}_p = 12.8$ m/s for the nozzle of $\alpha = 30°$ is about 2.4% higher than that for the nozzle of $\alpha = 0°$ and 5% higher than that for the nozzle of $\alpha = 90°$. This result implies that the air spiral flow from the nozzle of $\alpha = 30°$ makes slightly larger particle-averaged axial velocity. About 100 frames are used to get the particle samples of $n = 120$ in the statistical calculation. The particle-averaged velocity is not changed when more frames are used.

Measurement for the case of an increased particle load needs in addition an algorithm for the particle identification. The 4-PTV [18] is a possible method for this purpose. The 4-PTV demands longer axial length of the measurement region for four-frame tracking instead of two-frame tracking. Referring to Fig. 8, calculation of particle pair identification is carried out by the following equations:

$$\sigma_t = \sqrt{\frac{\sigma_l^2}{d_m^2} + \sigma_\theta^2}, \tag{9}$$

where:

$$d_m = \frac{1}{3}(d_{ij} + d_{jk} + d_{kl}), \qquad \theta_m = \frac{1}{2}(\theta_{ik} + \theta_{jl}), \tag{10}$$

$$\sigma_l = \sqrt{\frac{1}{3}\left(|d_{ij} - d_m|^2 + |d_{jk} - d_m|^2 + |d_{kl} - d_m|^2\right)}, \tag{11}$$

$$\sigma_\theta = \sqrt{\frac{1}{2}\left(|\theta_{ik} - \theta_m|^2 + |\theta_{jl} - \theta_m|^2\right)}. \tag{12}$$

As shown in Fig. 8, x_i, x_j, x_k and x_l are regarded as the coordinates of the same particle in four consecutive frames when the value of evaluation function σ_t takes a minimum value. As an example, a vector map of particle velocities obtained from the 4-PTV technique is plotted in the axial coordinate x and the vertical coordinate z as shown in Fig. 9.

3.4. Probability distributions of particle locations

Probability distributions of particle locations are determined by using the 2-PTV technique [20]. The

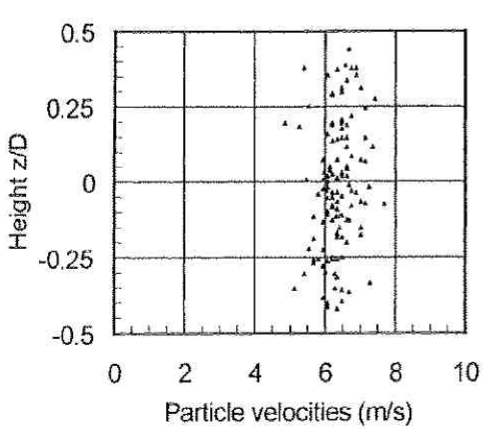

a. $x/D=20$, $\bar{u}_p = 6.3$ m/s

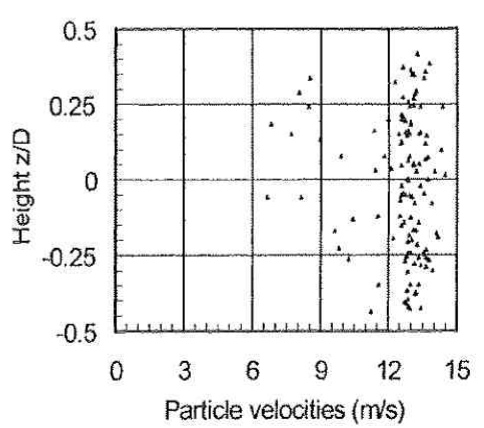

b. $x/D=200$, $\bar{u}_p = 12.5$ m/s

Fig. 5. Particle axial velocities for the nozzle of $\alpha = 0°$.

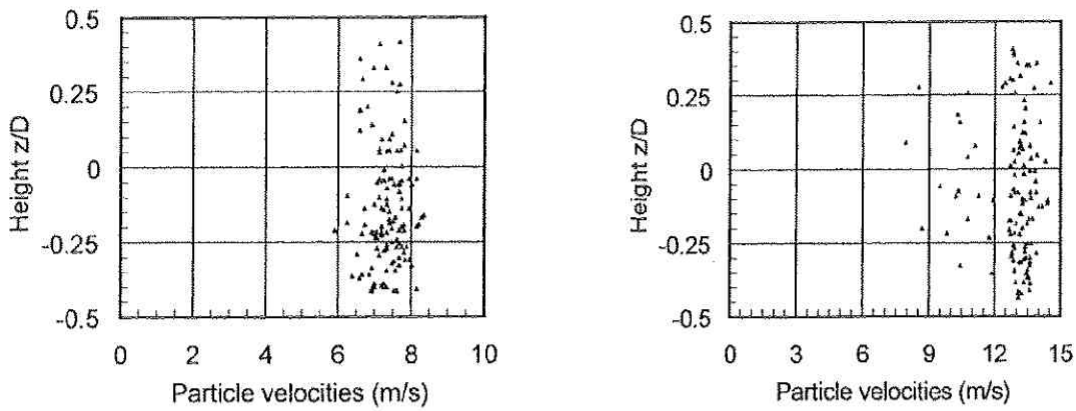

Fig. 6. Particle axial velocities for the nozzle of $\alpha = 30°$.

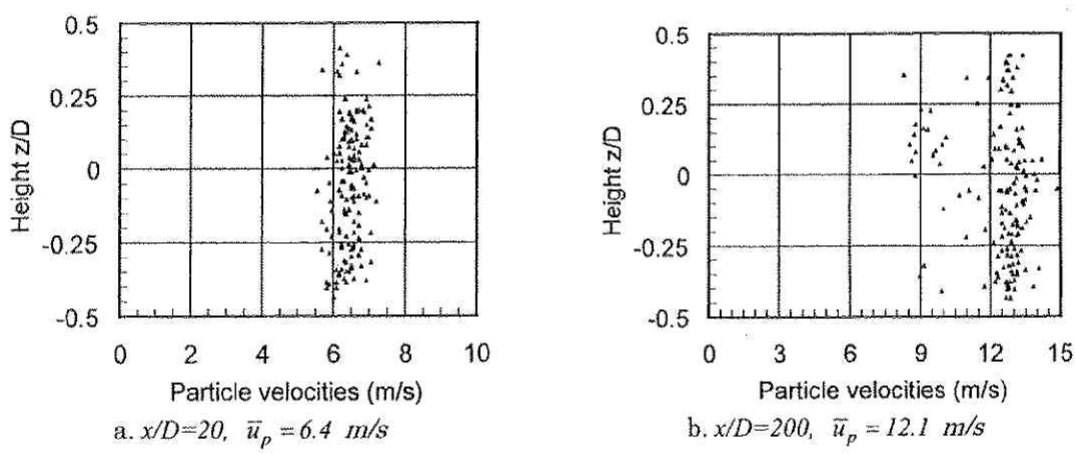

Fig. 7. Particle axial velocities for the nozzle of $\alpha = 90°$.

measurement section was divided into several sub-regions in a pipe cross-section to observe the particle suspension. To describe macroscopic features of particle transversal migration, probabilities for a particle to appear in every sub-region are calculated according to the following equation:

$$E_{(i)} = \left(\sum_{j=1}^{m} N_{ji} \Big/ N_{mt} \right) \times 100\%, \quad i = 1, 2, \ldots, i_m, \qquad (13)$$

where N_{mt} is total particle number of m frames, N_{ji} is particle number in the sub-region i of the jth frame, and the measurement sections in every frame are divided into the i_m sub-regions.

In this analysis, the pipe cross-section is divided into three sub-regions in the radial direction, i.e. $i_m = 3$ in Eq. (13). Every sub-region has an equal area of $\pi D^2/12$ (allowing for a comparison of the probability density). The first is the pipe center region of $2r/D < 0.577$. The second is the region of $0.577 \leqslant 2r/D < 0.816$. The third is the region of $0.816 \leqslant 2r/D < 1.0$. Here r is the radial distance from a particle location to the pipe axis. Measurement results of probability distributions of particle locations are given in Figs. 10–12.

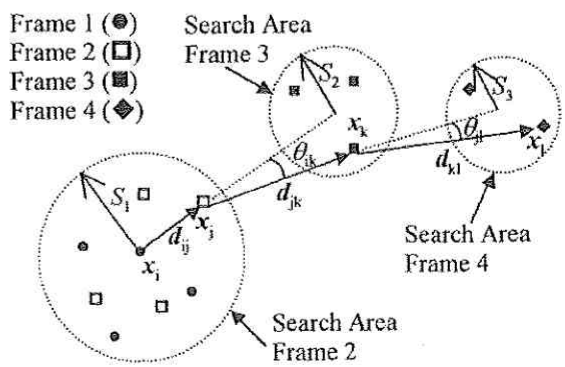

Fig. 8. Schematic diagram of the 4-PTV algorithm [18].

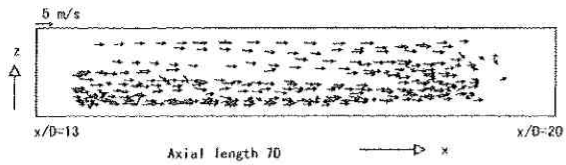

Fig. 9. A velocity vector map in the x–z plane for the nozzle of $\alpha = 30°$.

In the section of $x/D = 20$ for all the three nozzles of $\alpha = 30°$, 60° and 90° smaller probabilities are found in the regions near the pipe wall, while most particles are located in the region of $2r/D < 0.816$. The result indicates that particles tend to migrate towards pipe center and the particle–pipe friction may be decreased by the spiral flow. From this viewpoint, the nozzle of $\alpha = 30°$ achieves the best result among the three nozzles, i.e. minimum probability in the near wall region, among the three nozzles.

In the measurement cross-section at $x/D = 200$ where the nozzle effect is decreased, particle probability densities in the regions near the pipe wall increase for all the three nozzles. Compared with the nozzles of $\alpha = 0°$ and 90°, the nozzle of $\alpha = 30°$ results in lower probability density in the region near the pipe wall, and may make fewer particle–pipe collisions.

3.5. Errors in the experiment

Measurement errors of velocity vectors happen throughout the whole experimental process of PIV. The first is the resolution error of the particle displacement due to the CCD camera sampling of the particle images. The error in the particle displacement is $\sqrt{2}$ times the particle centroid error, which is a function of parameters depending on the image particle radius, the pixel size, and the Gaussian peak location on the CCD array, etc. According to research of Veber et al. [25], a referential estimation of the error is about $\pm\sqrt{2}/3$ pixel for a particle image with about 15 pixels in our experiment. The averaged displacement of particles in the axial direction traveled by the particles between two consecutive pic-

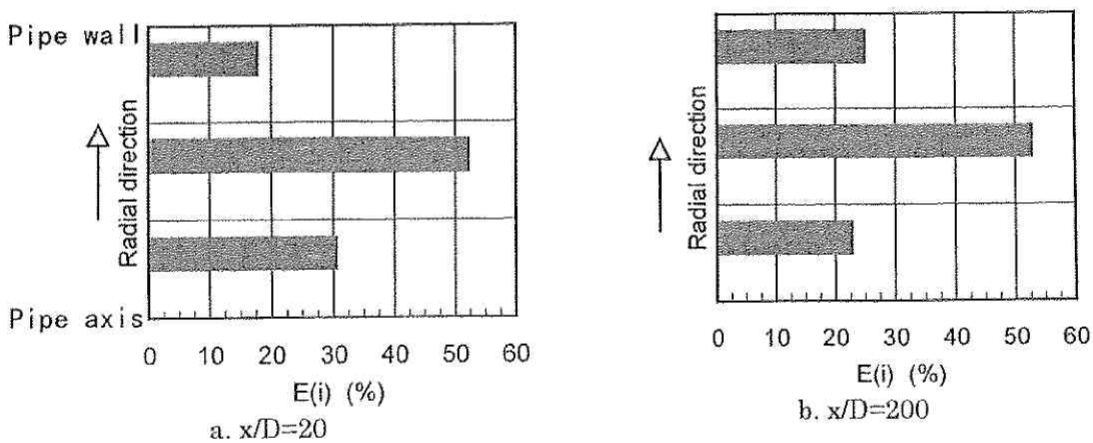

Fig. 10. Probability distribution of particle locations for the nozzle of $\alpha = 0°$.

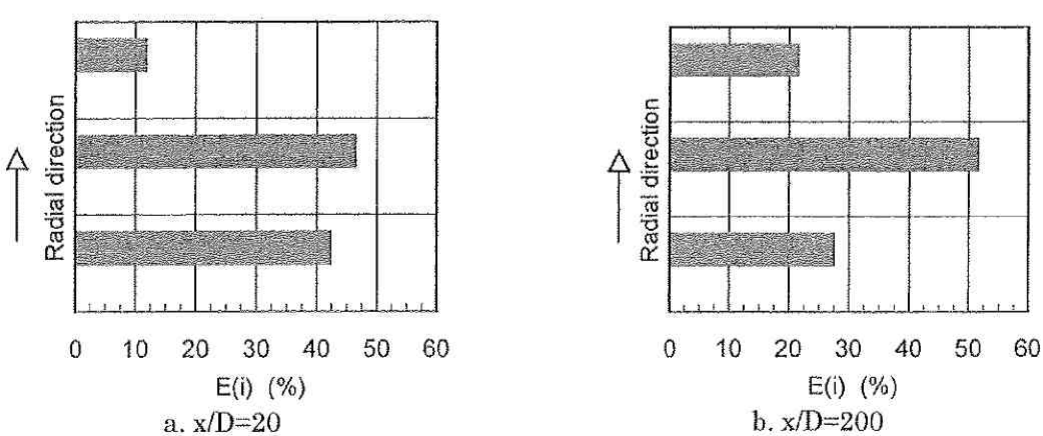

Fig. 11. Probability distribution of particle locations for the nozzle of $\alpha = 30°$.

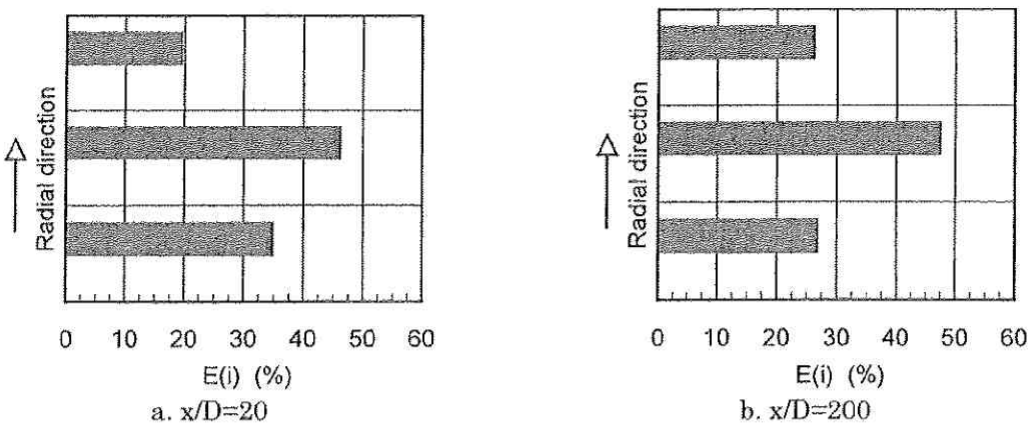

Fig. 12. Probability distribution of particle locations for the nozzle of $\alpha = 90°$.

tures is about 90 pixels. The resolution error due to CCD camera sampling is about ±0.5%. However, the averaged displacements in the y- and z-directions covered by the particles between two consecutive pictures are only about 1.5 and 2 pixels, respectively. Corresponding resolution errors then reach ±31% and ±25%, respectively. Inaccuracies of the radial and azimuthal velocities are therefore much larger than that of the axial velocity. This is the reason why we fail to obtain reliable radial and azimuthal velocities for the particle motion in this transportation system.

Another error may be caused by calibration of camera parameters and frame grabber. Camera parameters may be well calibrated and corresponding error is neglected. However, the selection of the threshold level, which depends on the operator, may produce inaccuracy. The size of the particle image decreases as the level of the threshold increases. This kind of inaccuracy may reach ±1/4 pixel. This error may not be important for the measurement of the axial velocity, but should be important for the measurement of the radial and azimuthal velocities. A total inaccuracy may reach $\pm(1/4 + \sqrt{2}/3)$ pixel, and this estimation shows that the total inaccuracy of the axial velocity reaches 1.6%. PIV is basically efficient in the measurement of particle axial velocity for transportation pipeline . However, it is difficult to measure the radial and azimuthal components of velocities with high accuracy, because they are much smaller than the mean axial velocity.

4. Practical significance

It is shown that PIV techniques are useful for the measurement of particle axial-velocities and particle locations in pipe cross-sections for the problem of pneumatic transportation of solid particles in a pipeline. This study reveals the mechanism of the high-efficiency transportation of the spiral flow, and makes the spiral flow applicable to practical systems.

5. Conclusions

The features and classification of PIV are discussed in detail in Section 2. An emphasis is laid on the algorithms for particle pair identification. It is shown that most PIV algorithms are limited to low particle number density. Algorithms for high particle number density in three-dimensional flows need to be developed. The PIV techniques have been applied to measure particle motion in a spiral gas–solid two-phase flow. Low probability densities of particle locations in the region near the pipe wall are found and show that the spiral flow can decrease particle–pipe contact. This is an important reason for reduction of power consumption when the spiral nozzle is used. It is also shown that the PIV techniques can measure the particle axial velocities with high accuracy but have difficulty in simultaneous measurement of the radial and azimuthal velocities.

Nomenclature

A_{fg}	a similarity coefficient based on the quadratic differences of gray levels (dimensionless)
B_{fg}	a similarity coefficient based on absolute values of differences of gray levels (dimensionless)
C_{fg}	cross-correlation coefficient (dimensionless)
$C_{f-\bar{f}g-\bar{g}}$	cross-correlation coefficient calculated based on brightness difference (dimensionless)
D	pipe diameter (m)
d_{ij}	length of the displacement vector of particle location from x_i to x_j in the 4-PTV algorithm (m)
d_{jk}	length of the displacement vector of particle location from x_j to x_k in the 4-PTV algorithm (m)

d_{kl}	length of the displacement vector of particle location from x_k to x_l in the 4-PTV algorithm (m)
$E_{(i)}$	probability of particle locations (dimensionless)
MA	magnification (dimensionless)
r	distance from particle location to pipe axis (m)
T	a similarity coefficient calculated based on the Delaunay triangle (dimensionless)
$\bar{u}_p$	averaged axial velocity of particles (m/s)
x, y, z	Cartesian coordinates (m)
$y(p)$	y-coordinate of the particle p (m)
$y1(p)$	y-coordinate in the mirror (m)

Greek symbols

α	slit angle of the spiral nozzle (degree)
Δt	time interval between two frames (s)
θ_{ik}	angle between the vectors of d_{ij} and d_{jk} (rad)
θ_{jl}	angle between the vector of d_{jk} and that of d_{kl} (rad)

Acknowledgements

The authors would like to express their thanks to Mr. T. Shomen, and Mr. K. Oyaizu, who were students at Fukui University, for their energetic help in the experiment.

References

[1] R.J. Adrian, Particle-imaging techniques for experimental fluid mechanics, Ann. Rev. Fluid Mech. 23 (1991) 261–304.

[2] C. Willert, M. Raffel, J. Kompenhans, B. Stasicki, C. Kähler, Recent applications of particle image velocimetry in aerodynamic research, Flow Meas. Instrum. 7 (1996) 247–256.

[3] M. Raffel, J. Kompenhans, Theoretical and experimental aspects of image-shifting by means of a rotating mirror system for particle image velocimetry, Meas. Sci. Technol. 6 (1995) 795–808.

[4] R.J. Adrian, Bibliography of particle velocimetry using imaging methods: 1917–1995. TAM Report No. 817, University of Illinois at Urbana-Champaign, 1996.

[5] P.E. Dimotakis, F.D. Debussy, M.M. Koochesfahani, Particle streak velocity field measurements in a two-dimensional mixing layer, Phys. Fluids 24 (1981) 995–999.

[6] B. Khalighi, Study of the intake swirl process in an engine using flow visualization and particle tracking velocimetry, ASME-FED 85 (1989) 37–47.

[7] P.G. Simpkins, T.D. Dudderar, Laser speckle measurement of transient Bénard convection, J. Fluid Mech. 89 (1978) 665–671.

[8] M. Kawahashi, K. Yamamoto, Speckle method using beam scanning techniques, Proceedings of the International Workshop on PIV-Fukui'95, Visual. Soc. Japan, 1995, pp. 155–158.

[9] L.C. Gui, W. Merzkirch, A method of tracking ensembles of particle images, Exp. Fluids 21 (1996) 465–468.

[10] A. Kaga, Y. Inoue, K. Yamaguchi, Pattern tracking algorithms for airflow measurement through digital image processing of visualized images, J. Visual. Soc. Jpn. 14 (1994) 38–45.

[11] T. Uemura, F. Yamamoto, M. Koukawa, High-speed algorithm for particle tracking velocimetry using binary, J. Visual. Soc. Jpn. 10 (1990) 196–202.

[12] F. Yamamoto, A. Wada, M. Iguchi, M. Ishikawa, Visualization and image processing of torque converter internal flow, J. Flow Visualization Image Processing 3 (1996) 51–64.

[13] F. Yamamoto, A. Wada, M. Iguchi, M. Ishikawa, Discussion of the cross-correlation methods for PIV, J. Flow Visualization Image Processing 3 (1996) 65–78.

[14] X. Song, F. Yamamoto, M. Iguchi, Y. Murai, A new tracking algorithm of PIV and removal of spurious vectors using Delaunay tessellation, Exp. Fluids 26 (1999) 371–380.

[15] K. Okamoto, Three-dimensional particle tracking algorithms: velocity vector histogram and spring model, Proceedings of the International Workshop on PIV-Fukui'95, Visual. Soc. Japan, 1995, pp. 21–32.

[16] M. Ishikawa, F. Yamamoto, Y. Murai, M. Iguchi, A. Wada, A novel PIV algorithm using velocity gradient tensor, Proceedings of the Second International Workshop on PIV'97-Fukui, Visual. Soc. Japan, 1997, pp. 51–56.

[17] S.J. Baek, S.J. Lee, A new two-frame particle tracking algorithm using match probability, Exp. Fluids 22 (1996) 23–32.

[18] N. Nishino, N. Kasagi, M. Hirata, Three-dimensional particle tracking velocimetry based on automated digital image processing, Trans. ASME J. Fluids Eng. 111 (1989) 384–391.

[19] N.A. Malik, Th. Dracos, D.A. Papantoniou, Particle tracking velocimetry in three-dimensional flows, Part II: Particle tracking, Exp. Fluids 15 (1993) 279–294.

[20] Z.C. Liu, R. Adrian, Simultaneous imaging of the velocity fields of two phases, in: M.C. Roco (Ed.), Particulate Two-Phase Flow, Butterworths/Heinemann, London,1996, pp. 33–58.

[21] M.P. Wernet, A. Pline, Particle displacement tracking technique and Cramer-Rao lower bound error in centroid estimates from CCD imagery, Exp. Fluids 15 (1993) 295–307.

[22] J. Westerweel, Efficient detection of spurious vectors in particle image velocimetry data, Exp. Fluids 16 (1994) 236–247.

[23] H.T. Huang, H.E. Fiedler, J.J. Wang, Limitation and improvement of PIV, Part I: Limitation of conventional techniques due to deformation of particle image patterns, Exp. Fluids 15 (1993) 168–174.

[24] H.T. Huang, H.E. Fiedler, J.J. Wang, Limitation and improvement of PIV, Part II: particle image distortion, a novel technique, Exp. Fluids 15 (1993) 263–273.

[25] P. Veber, J. Dahl, R. Hermansson, Study of the phenomena affecting the accuracy of a video-based particle tracking velocimetry technique, Exp. Fluids 22 (1997) 482–488.

[26] K. Horii, Using spiral flow for optical cord passing, ASME Mech. Eng. 112 (1990) 68–69.

[27] K. Horii, Y. Matsumae, X.M. Cheng, M. Takei, E. Yasukawa, B. Hashimoto, Focusing phenomenon and stability of spiral air jet, Trans. Jpn. Soc. Aero. Space Sci. 33 (1991) 141–153.

[28] K. Horii, Y. Matsumae, X.M. Cheng, M. Takei, B. Hashimoto, A study of spiral flow (Part 3): Opening and orientation control of fiber by spiral nozzle, Trans. Jpn. Soc. Aero. Space Sci. 32 (1990) 155–183.

[29] K. Horii, Y. Matsumae, X.M. Cheng, M. Takei, B. Hashimoto, A study of spiral flow (Part 4): The effect of radial Reynolds number of spiral flow on plasma deposition of pipe, Trans. Jpn. Soc. Aero. Space Sci. 32 (1990) 165–175.

[30] K. Horii, H. Sawazaki, Y. Matsumae, X.M. Cheng, M. Takei, E. Yasukawa, B. Hashimoto, New continuous system for dispersion and encapsulation of submicron powders using spiral flow, ASME FED 100 (1990) 25–30.

[31] K. Horii, Y. Matsumae, K. Ohsumi, X.M. Cheng, S. Kage, B. Hashimoto, Novel optical fiber installation by use of spiral airflow, ASME J. Fluids Eng. 114 (1992) 375–378.

[32] K. Miyazaki, G. Chen, M. Miyazaki, F. Yamamoto, K. Ohsumi, K. Horii, High performance slurry transportation for sewage pipe installation, Proceedings of the International Conference on Trenchless Tech., Int. Soc. Trenchless Tech. 5B-3-1, 1997.

[33] S. Murai, H. Nakamura, Y. Suzaki, Analytical orientation for non-metric camera in the application to terrestrial photogrammetry, Int. Arch. Photogramm 23 (1980) 516–525.